An Analytical Model for Internal Moisture Content During the Decreasing Drying Rate Period

L. Derdour
AstraZeneca Process R&D, 15185 Södertälje, Sweden

H. Desmorieux
Laboratoire d'Automatique et de GÉnie des Procédés, LAGEP UPRES-A CNRS
Q5007-Université Claude BERNARD LYON-I CPE - bat. 308, 43,
Bd du 11 novembre 1918, 69622 Villeurbanne Cédex, France

DOI 10.1002/aic.11370
Published online December 26, 2007 in Wiley InterScience (www.interscience.wiley.com).

A system of analytical expressions for internal moisture distribution during the falling drying rate period for porous nonhygroscopic slabs is presented. This model is derived by resolution of thermal balance and mass flux continuity equations and on the assumption of a parabolic internal moisture profile in the liquid transport zone. This study is based on the assumption of the existence of a receding evaporative front within the product during the decreasing drying rate period and on heat transfer being the limiting mechanism. The model addresses the cases where heat transfer is the limiting mechanism during drying and applies to flat slabs which are classified into two groups, namely, thick products and thin products, depending on their thicknesses and drying conditions. Overall, the model predictions were in a slight deviation from experimental data obtained on plaster. © 2007 American Institute of Chemical Engineers *AIChE J,* 54: 475–486, 2008

Keywords: separations, moisture content profile, modeling, evaporative front, convective drying

Introduction

Prediction of internal moisture content evolution during drying is very important for determining drying kinetics. The knowledge of drying kinetics is necessary for good control of product quality and optimal dryer selection and drying operation. In the pharmaceutical industry, regulatory bodies impose obtaining active pharmaceutical ingredients with uniform internal solvent content making the knowledge of residual solvent distribution a prerequisite before conducting any product quality performance and process validation studies as mentioned by Bindschaedler.[1] In contrast, final residual solvent profile has a proven effect on the activity and the stability of active ingredients and therefore, it must be carefully monitored and controlled (see May[2]). Knowledge of the internal solvent gradient is a valuable information for drying process scale-up and implementation. For example, in the pharmaceutical industry, it is important to know if there are significant solvent moisture content gradients during the drying of a less stable crystalline or amorphous form of an active pharmaceutical ingredient, because high levels of residual solvent is known to enhance molecular mobility, which favors solid state transitions as mentioned by Hancock and Zografi.[3] Consequently, knowledge of internal solvent/moisture distribution is very valuable in the implementation of robust drying cycles that will produce consistently the desired polymorphic variety.

Prior Work

The importance of internal moisture distribution explains the large number of papers and books devoted to its study and to drying kinetics prediction like the works of Martynenko

Correspondence concerning this article should be addressed to L. Derdour at Lotfi.Derdour@astrazeneca.com.

et al.,[4] Keey,[5] Schlünder,[6] and Van Brakel.[7] Recently, Coumans[8] published a paper in which he classifies the drying model into three major groups, namely, the general models, the lumped diffusion models, and the receding front models. The general models are empirical in nature and rely on information extracted from experiments, the lumped diffusion models consider an equivalent diffusion coefficient that gathers all the contributing mass transfer mechanisms occurring during drying for simplification. Finally, the receding front models assume the formation of a dry zone in the product during the falling drying rate period. This zone represents a supplementary resistance to mass transfer, which contributes to the decrease of the drying rate. So far, three major causes were presented to explain the drop in the drying rate just after the constant drying rate period (CDRP), when it exists. The first explanation is that the external surface from which evaporation occurs is no longer saturated and starts showing dry patches. The surface allowed for evaporation is then reduced leading to a decrease in the drying rate. Belhamri[9] has recently examined this theory and found out that the external surface remains saturated up to 80% until the critical moisture content is reached then it starts dropping. This result works against the apparition of dry patches explanation. The second explanation of the fall of the drying rate is the drop in the internal mass transfer which becomes insufficient to compensate the moisture loss at the external surface. Despite the extensive literature dedicated to drying research and development spanned over a period of a century, this theory has not been proved explicitly. The third explanation is the formation of a dry zone and that the evaporation occurs inside the product during the falling drying rate period. Recently, many authors used this model successfully, particularly for capillary-porous materials: Derdour and Desmorieux[10] developed a model that assumes a minimal for the liquid diffusion coefficient at the receding evaporative front, Pel and Landman[11] presented a similar model that relies on experiments to evaluate many adjustment parameters needed by the model. However, no straightforward analytical model has been presented that gives access to many variables without extensive numerical resolution or experimentation. In the prior work, most investigators approached drying modeling and internal moisture profiles determination by considering a global equivalent moisture diffusion coefficient. The dependence of that coefficient was then adapted to each drying scenario usually with the help of experimental data. A compilation of the prior work up to 1995 can be found in a review by Marinos-Kouris and Maroulis.[12] A review of the main approaches for drying modeling has also been recently presented by Chen and Wang.[13] The most frequent expressions of the diffusion coefficient are the Arrhenius relationship and the polynomial expression which lacks strong theoretical foundations. Therefore, only few analytical expressions for the internal moisture distributions during the decreasing drying rate period (DDRP) were determined in the literature for specified conditions as the ones obtained by Crank[14] and Moyne et al.,[15] among others. Most authors including De vries,[16] Luikov,[17] Peishi Chen and Pei,[18] and Schadler and Kast,[19] considered the mass transfer as having an equal or higher effect on the drying process than heat transfer. However, if the product has a capillary-porous structure, resistance to mass transfer is reduced while resistance to heat transfer is higher than in dense materials.

This article addresses the cases where heat transfer is the limiting mechanism during the falling drying rate period, which is the case of drying under reduced pressure as reported by King[20] and Rey.[21] Heat transfer can also be the limiting mechanism during drying of porous materials with relatively large pore sizes as stated by Mujumdar and Menon.[22] This is explained by the fact that during the falling drying rate period of porous bodies when a porous dry zone is created, pores get filled with the drying agent. This is expected to increase the gaseous molecular diffusion and decrease heat transfer effective conductivity in the dry zone. For convective drying, literature provides very few drying models for cases where heat transfer can be considered as the limiting mechanism. This article provides a brief analysis of the limiting mechanism during drying, an analytical model for the cases where heat transfer governs drying and a comparison of the model's predictions with experimental data obtained on plaster.

Mathematical Modeling

The model presented in this article addresses the case where heat transfer is the limiting mechanism during the falling drying rate period, which is likely to occur for capillary-porous bodies. The model presented in this study is based on simplifying hypotheses and provides a complete representation of the drying of capillary-porous materials. The model resolution needs the availability of the product characteristics such as the thermal conductivity, the initial moisture content, the density, the product thickness, the internal moisture diffusivity which can be determined using a single experiment. The drying conditions are also needed by the model. Predictions of the model presented in this article are compared with experimental data obtained on plaster. This material has a capillary-porous internal structure that satisfies the assumption of heat transfer being the limiting mechanism during the falling drying rate period.

In a previous paper (Derdour et al.[23]), we examined the theoretical foundations of the characteristic drying curve (CDC) concept and derived a model to represent experimental CDC's for porous nonhygroscopic slabs. In this article, this model is developed further to obtain the following analytical relationships:

- The mean moisture content in the product vs. the dry zone normalized thickness;
- The local moisture content vs. the dry zone normalized thickness;
- Time vs. the dry region normalized thickness. This relationship combined with the two mentioned above, yields respectively the mean moisture content vs. time, the local moisture content vs. time and the spatial coordinate;
- The expression of the diffusional region thickness as a function of the dry zone normalized thickness during the penetration period.

This model is applicable for capillary-porous nonhygroscopic slabs that are classified into thin and thick products depending on the product thickness and drying conditions (see Derdour et al.[23,24]). Its validity was examined by comparing its predictions to experimental data obtained with drying of plaster slabs.

The model presented in this article is based on some assumptions, which were in most cases verified by experimen-

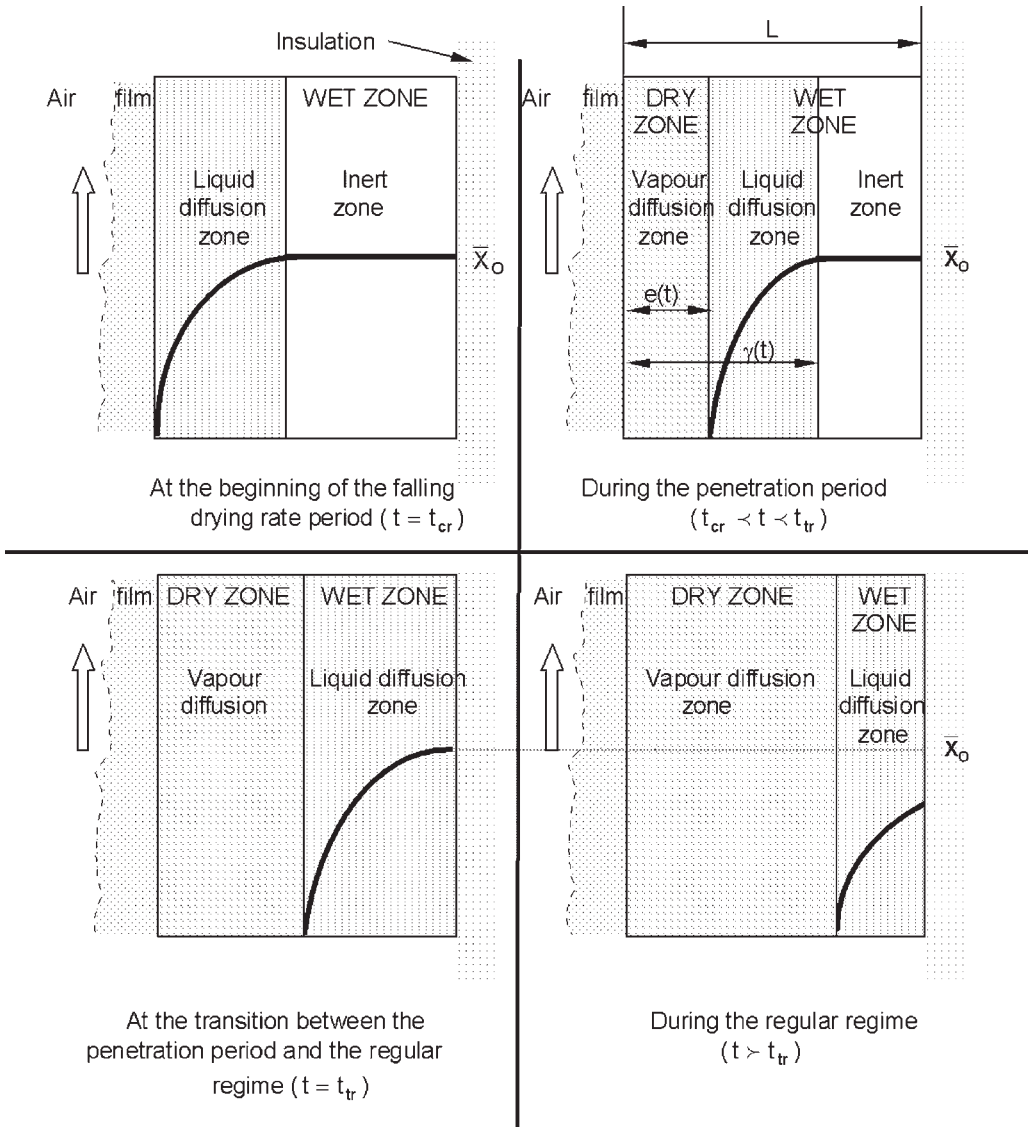

Figure 1. Evolution of internal moisture content distribution during the DDRP for thick products.

tal results obtained on plaster-based products. The main assumptions of this study are as follows:

- Heat transfer is the limiting mechanism of the process, that is, the amount of vapor generated at the receding evaporative front is less than the amount of vapor that can be transferred through the dry region and the external film;
- In the wet zone of the capillary-porous structure, the main mass transport mechanism is liquid transport by capillarity. However, Keey[5] and Marino-Kouris and Maroulis,[12] among many other authors, state that capillarity can be represented by a diffusion-type equation. In this article, internal liquid transport is assumed to follow a diffusion pattern with a constant equivalent diffusivity. As a consequence, the internal moisture content profile in the wet zone can be considered parabolic (Keey[5] and Crank[14]). Experimental evidence obtained on capillary-porous material similar to plaster indicates that the average moisture diffusivity is approximately constant (Derdour and Desmorieux[10] and Derdour et al.[25]). In the dry region, vapor molecular diffusion through pores filled with air is assumed to occur. Constant vapor diffusion coefficient is assumed and Knudsen diffusion is neglected because of the relative large size of the pores. Vapor generated is considered as an ideal gas;
- Evaporation is instantaneous, that is, it is not a slow process that can limit transport phenomena. It can be described by a Clausius–Clapeyron type relationship and takes place only at a receding evaporative front within the product during the falling rate period. This front separates the dry zone from the wet zone and moves toward the bottom of the product during drying. As a result, the thickness of the dry zone, $e(t)$, broadens at the expense of the wet zone during the process (cf. Figure 1). For porous products such as plaster-based slabs, the existence of the internal receding evaporative front was verified experimentally by Derdour[24];
- Products are classified into two groups, namely, thick products and thin products. The transitional thickness between these two groups depends on material properties (physicochemical properties, thickness, moisture diffusivity) and on

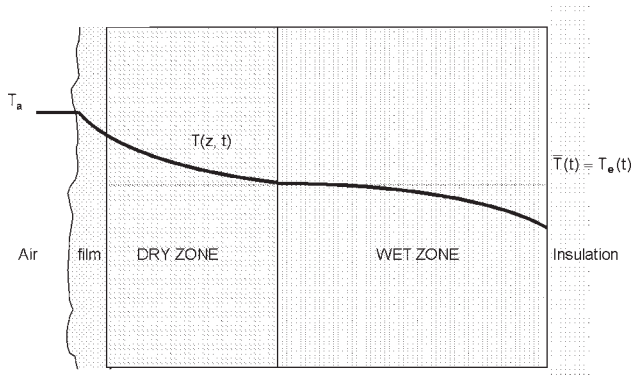

Figure 2. Assumed internal temperature profile during the falling drying rate period.

external drying conditions (drying rate during the CDRP). The product is considered as thin if the internal moisture profile at the critical moisture content is parabolic all across the product. In this case, the entire falling drying rate period corresponds to the so called regular regime. If at the end of the CDRP, there is still a part of the product located by its core and remaining at the initial moisture content, the product is considered as a thick one and the DDRP follows two subperiods: the penetration period followed by the regular regime. During the penetration period, the liquid diffusion advances toward the bottom of the product and the regular regime begins once liquid diffusion reaches the core of the material. Typical evolution of the internal moisture distribution for a thick product is illustrated on Figure 1.

The other assumptions for the presented model are as follows:

- The temperature at the receding evaporative front is approximately equal to the mean product temperature (cf. Figure 2);
- The interface between the wet zone and the dry zone is assumed to be pseudo-saturated and the heat of vaporization is considered constant in the range of temperatures considered in this study;
- The product is porous, nonhygroscopic and has a flat form. The air is in contact only with the upper face, all other faces are isolated. With this configuration, heat and mass transfer can be considered as unidirectional and heat losses can be neglected.

The assumptions stated above hold for products having a capillary structure and large pores such as plaster, which is used as a test product in this study. For products proven to have variable transport coefficients, the model presented in this article can not be used in its current form but has to be modified to take into consideration the variable transport properties. In that case, the analytical resolution of the balance and continuity equations might be impossible to achieve and the theoretical internal moisture distributions can only be determined with the help of numerical methods for a given set of drying conditions. However, the model presented in this article can be further developed to predict drying kinetics for hygroscopic slabs by introducing the sorption isotherm and the equilibrium moisture content.

With the help of the assumptions listed earlier, we will analyze the transport mechanisms and properties to determine the conditions that favor heat transfer being the limiting mechanism. Then, knowing the boundary conditions and the equations resulting from the global thermal balance and the mass flux continuity, we can determine the relationships giving the internal moisture content distribution during the DDRP.

Simplified analysis of the limiting mechanism during drying

During the DDRP, the heat transferred from air to the product is used to evaporate moisture at the receding evaporative front and to increase the product temperature. Hence, we define the fraction of the heat used to heat the material:

$$q = \frac{Q_{\text{prod}}}{Q_{\text{trans}}} \tag{1}$$

The heat transferred from air to the product is the sum of the heat used to increase the product temperature and the heat used to evaporate moisture:

$$Q_{\text{trans}} = Q_{\text{prod}} + Q_{\text{evap}} \tag{2}$$

The sensible heat term Q_{prod} is 40 times less than the water evaporative heat term Q_{evap} so that Eq. 2 can be reduced to (Keey and Suzuki[26]):

$$Q_{\text{trans}} = Q_{\text{evap}} \tag{3}$$

Since the sensible heat is negligible, a pseudo-stationary state for heat transfer in the dry zone can be assumed. Therefore, the heat flux passing through the dry zone can be expressed as follows:

$$Q_{\text{ev}} = \frac{1}{\frac{1}{h} + \frac{e(t)}{\lambda_{\text{dr}}}} (T_{\text{a}} - T_{\text{e}}(t)) \tag{4}$$

Instantaneous evaporation allows writing:

$$Q_{\text{ev}} = (\dot{m})_{\text{ht}} L_{\text{v}} \tag{5}$$

where $(\dot{m})_{\text{ht}}$ is the vapor generation rate, that is, mass flux produced at the receding evaporative front as a result of heat transfer.

Introducing the heat Biot number:

$$Bi_{\text{c}} = \frac{hL}{\lambda_{\text{dr}}} \tag{6}$$

and the normalized thickness of the dry zone:

$$\xi(t) = \frac{e(t)}{L} \tag{7}$$

Eq. 5 becomes:

$$(\dot{m})_{\text{ht}} = \frac{1}{1 + Bi_{\text{c}}\ \xi(t)} \frac{h}{L_{\text{v}}} (T_{\text{a}} - T_{\text{e}}(t)) \tag{8}$$

In contrast, assuming a pseudo-steady state, the amount of vapor that can be transported through the dry zone and the external film can be expressed as:

$$(\dot{m})_{\text{mt}} = \frac{k}{1 + Bi_{\text{m}} \xi(t)} (C_{\text{ve}}(t) - C_{\text{va}}) \tag{9}$$

where Bi_{m} is the mass Biot number:

$$Bi_{\text{m}} = \frac{kL}{D_{\text{ev}}} \tag{10}$$

To compare the evaporation rate, that is, source of mass flux generated following heat transfer to mass transfer through the

dry zone and the external film, we introduce the dimensionless number Γ as:

$$\Gamma = \frac{(\dot{m})_{\mathrm{mt}}}{(\dot{m})_{\mathrm{ht}}} \tag{11}$$

Γ is used to compare the vapor generation rate at the receding evaporative front to the mass flux that can be transferred through the dry region and the external film Values of Γ lower than 1 indicate that mass transfer is the limiting mechanism. Conversely, values of Γ higher than unity will indicate that heat transfer governs the drying kinetics.

Substitution of Eqs. 8 and 9 in Eq. 11 yields:

$$\Gamma = \frac{kL}{h}\left(\frac{1+Bi_{\mathrm{c}}\xi(t)}{1+Bi_{\mathrm{m}}\xi(t)}\right)\left(\frac{C_{\mathrm{ve}}(t)-C_{\mathrm{va}}}{T_{\mathrm{a}}-T_{\mathrm{e}}(t)}\right) \tag{12}$$

During the CDRP, mass flux is expressed as:

$$\dot{m}_{\mathrm{l}} = k(C_{\mathrm{vs}} - C_{\mathrm{va}}) \tag{13}$$

Using heat balance during the CDRP, mass flux can also be expressed as:

$$\dot{m}_{\mathrm{l}} = \frac{h}{L_{\mathrm{v}}}(T_{\mathrm{a}} - T_{\mathrm{w}}) \tag{14}$$

Assuming using dry air ($C_{\mathrm{va}} = 0$), substitution of Eqs. 13 and 14 in Eq. 12 yields:

$$\Gamma = \left(\frac{1+Bi_{\mathrm{c}}\xi(t)}{1+Bi_{\mathrm{m}}\xi(t)}\right)\left(\frac{T_{\mathrm{a}}-T_{\mathrm{w}}}{C_{\mathrm{vs}}}\right)\left(\frac{C_{\mathrm{ve}}(t)}{T_{\mathrm{a}}-T_{\mathrm{e}}(t)}\right) \tag{15}$$

We define the dimensionless numbers:

$$\Psi = \frac{1+Bi_{\mathrm{c}}\xi(t)}{1+Bi_{\mathrm{m}}\xi(t)} \tag{16}$$

and

$$\Omega = \left(\frac{T_{\mathrm{a}}-T_{\mathrm{w}}}{C_{\mathrm{vs}}}\right)\left(\frac{C_{\mathrm{ve}}(t)}{T_{\mathrm{a}}-T_{\mathrm{e}}(t)}\right) \tag{17}$$

Analysis of Ω shows that it is equal to unity at the beginning of the DDRP During the DDRP, the Clausius–Clapeyron relationship between vapor pressure and temperature of evaporation is assumed to hold because evaporation takes place at a pseudo-saturated liquid front, thus the following approximation is valid:

$$P_{\mathrm{ve}}(t) = 1.013\times10^{5}\exp\frac{L_{\mathrm{v}}}{R}\left(\frac{1}{373.15}-\frac{1}{T_{\mathrm{e}}(\mathrm{t})+273.15}\right) \tag{18}$$

Besides vapor generated at the receding evaporative front is considered as an ideal gas, thus:

$$C_{\mathrm{ve}}(t) = \frac{P_{\mathrm{ve}}(t)M_{\mathrm{v}}}{RT_{\mathrm{e}}(t)} \tag{19}$$

During the DDRP, $T_{\mathrm{e}}(t)$ slowly increases and since $P_{\mathrm{ve}}(t)$ augments exponentially with $T_{\mathrm{e}}(t)$, the ratio $P_{\mathrm{ve}}(t)/T_{\mathrm{e}}(t)$ increases gradually (see Appendix, Figure A1 for the evolution of the ratio $P_{\mathrm{ve}}(t)/T_{\mathrm{e}}(t)$ for water between 20°C and 100°C). As a consequence, $C_{\mathrm{ve}}(t)$ and Ω are expected to increase during the DDRP. Therefore, the variation of Γ can be analyzed solely by examining the dependence of the dimensionless number Ψ upon drying conditions and product characteristics.

Heat transfer can be considered as the limiting mechanism with certainty if Ψ is higher than unity. For values of Ψ less than unity, no conclusion can be drawn as values of Γ will depend on the product (Ψ Ω).

Thus heat transfer is the limiting mechanism if:

$$\Psi = \frac{1+Bi_{\mathrm{c}}\xi(t)}{1+Bi_{\mathrm{m}}\xi(t)} > 0 \tag{20}$$

Equation 20 can be simplified further and finally, heat transfer can be considered as the limiting mechanism if the following condition is met:

$$\Lambda = \frac{hD_{\mathrm{ve}}}{k\ \lambda_{\mathrm{dr}}} > 1 \tag{21}$$

Therefore, conditions that favor most heat transfer being the limiting mechanism are drying under reduced pressure (high value of D_{ve}) of material of low thermal conductivity with large pore diameter (D_{ve} unaffected by internal porosity and high pore volume decreasing λ_{dr}). In the case where Λ is less than unity, one needs to calculate Γ during the DDRP to know which mechanism is limiting the process. Therefore, for highly porous materials as certain types of plaster, heat transfer can be considered as the limiting mechanism.

Model development

In a global approach with the simplifying assumption of a small internal temperature gradient (see Figure 2), the temperature at the receding evaporative front can be determined by expressing the variation of the material internal energy:

$$d(qQ_{\mathrm{trans}}) = dE_{\mathrm{int}} \tag{22}$$

where q represents the heat fraction used for heating the product

Considering parameters average values, Eq. 22 can be developed as follows:

$$qhA_{\mathrm{e}}(T_{\mathrm{a}} - T_{\mathrm{prod}}) = \rho_{\mathrm{prod}}V_{\mathrm{prod}}\mathrm{Cp}_{\mathrm{prod}}\frac{dT_{\mathrm{prod}}}{dt} \tag{23}$$

where $\mathrm{Cp}_{\mathrm{prod}}$ and T_{prod} represent the mean mass thermal capacity and the mean temperature of the product, respectively Finally, the analytic solution of Eq. 23 yields the temperature evolution at the receding evaporative front:

$$T_{\mathrm{e}}(t) \approx T_{\mathrm{prod}} = T_{\mathrm{a}} - (T_{\mathrm{a}} - T_{\mathrm{w}})\exp\left(-\frac{qh}{\rho_{\mathrm{prod}}\mathrm{Cp}_{\mathrm{prod}}L}t\right) \tag{24}$$

For the particular case of drying of capillary porous materials, that is, if the resistance to heat transfer is high, the temperature at the receding evaporative front is expected to increase slowly. Therefore, the analogy of Van Brakel[7] applies. It fallows during the DDRP, time is proportional to the square of the normalized thickness of the dry zone:

$$t = \alpha_{\mathrm{VB}}(\xi(t))^2 \tag{25}$$

Substitution of Eq. 25 in Eq. 24 yields:

$$T_{\mathrm{e}}(t) \approx T_{\mathrm{prod}} = T_{\mathrm{a}} - (T_{\mathrm{a}} - T_{\mathrm{w}})\exp\left(-\alpha[\xi(t)]^2\right) \tag{26}$$

where the coefficient α is defined as:

$$\alpha = \frac{qh\alpha_{\mathrm{VB}}}{\rho_{\mathrm{prod}}\mathrm{Cp}_{\mathrm{prod}}L} \tag{27}$$

α is assumed to be constant for a given material of a slab shape of a given thickness This parameter is related to the importance of heat transfer during the process. Low values of this parameter leading to a fraction of heat absorbed less than 0.1 indicate that mass transfer can be considered as the limiting mechanism. Values of α corresponding to a fraction of heat absorbed higher than 0.1 indicate that heat transfer is more likely to be the limiting step. For plaster slabs 0.03 m thick, α was found to be constant and equal to 12 by Derdour et al.[23] This value led to a fraction of heat absorbed by the product comprised between 0.1 and 0.35 indicating that heat transfer can be considered as the limiting transport mechanism.

Combining Eq. 8 with Eq. 14 yields:

$$\dot{m} = \frac{\dot{m}_l}{1 + Bi_c \xi(t)} \left(1 - \frac{T_e(t) - T_w}{T_a - T_w}\right) \tag{28}$$

Substitution of Eq. 26 in Eq. 28 gives the expression of the drying rate during the DDRP:

$$\dot{m} = \frac{\dot{m}_l \exp\left[-\alpha(\xi(t))^2\right]}{1 + Bi_c \xi(t)} \tag{29}$$

Equation 29 shows that for capillary-porous slabs, the drying rate during the falling drying rate period is function of α and Bi_c. In the case where resistance to internal heat transfer in the dry zone is high, that is, for low values of λ_{dr} and thus non-negligible values for Bic, Eq. 29 can be utilized to predict the drying rate during the falling drying rate period.

The diffusional model combined with the expression derived from the global thermal balance and the mass flux continuity relationship at the receding evaporative front, will determine the expressions relating the internal moisture distribution to time and spatial coordinate which is the main purpose of this article. For any given drying conditions, the transitional thickness between thick products and thin products can be deduced from the following expression obtained by Keey,[5] Derdour et al.,[25] and Suzuki[27]

$$L_{lim} = 2\rho_{dr} D_{le} \overline{X}_o / \dot{m}_l \tag{30}$$

This transitional thickness also depends on drying conditions and is not a constant for a given material.

The model developed in this article can be used for simulations knowing the product characteristics and drying conditions. The moisture diffusion coefficient D_{le} and Van Brakel's constant α_{VB} can be determined using a single drying experiment (Derdour[24]).

Modeling of the internal moisture content for thick products.

The Penetration Period. According to Fick's law, with a constant diffusion coefficient, the local moisture distribution can be considered as parabolic in the liquid diffusional region, then, the moisture distribution in the wet region is described by the following equations:

In the liquid diffusion region:

$$e(t) \le z \le \gamma(t), \quad X(z,t) = \overline{X}_o - a(t)(z - \gamma(t))^2 \tag{31}$$

In the inert region:

$$\gamma(t) \le z \le L, \quad X(z,t) = \overline{X}_o \tag{32}$$

At the receding evaporative front, the moisture content is equal to zero (cf. Figure 1), so that Eq. 31 gives:

$$a(t) = \frac{\overline{X}_o}{(e(t) - \gamma(t))^2} \tag{33}$$

Combining Eqs. 31 and 33 leads to:

$$X(z,t) = \overline{X}_o \left[1 - \frac{1}{L^2}\left(\frac{z - \gamma(t)}{\xi(t) - \gamma(t)/L}\right)^2\right] \tag{34}$$

With our hypotheses, the mean moisture content is expressed by the following equation:

$$\overline{X} = \frac{\overline{X}_o}{L}\left\{\int_{e(t)}^{\gamma(t)} \left[1 - \frac{1}{L^2}\left(\frac{z - \gamma(t)}{\xi(t) - \gamma(t)/L}\right)^2\right] dz + \int_{\gamma(t)}^{L} dz\right\} \tag{35}$$

This becomes, after few modifications:

$$\overline{X} = \frac{\overline{X}_o}{3}(3 - 2\ \xi(t) - \gamma(t)/L) \tag{36}$$

In contrast, the mass flux continuity at the receding evaporative front implies (application of the 1st Fick law):

$$\dot{m} = \rho_{dr} D_{le} \left.\frac{\partial X(z,t)}{\partial z}\right|_{z=e(t)} \tag{37}$$

Substitution of Eq. 34 in Eq. 37 yields:

$$\dot{m} = \frac{2\rho_{dr} D_{le} \overline{X}_o}{L} \frac{1}{\gamma(t)/L - \xi(t)} \tag{38}$$

Substitution of Eq. 29 in Eq. 38 gives an expression for the thickness of the diffusional region as a function of the dry zone normalized thickness:

$$\gamma(t) = L\xi(t) + \frac{2\rho_{dr} D_{le} \overline{X}_o}{\dot{m}_l}\left[\frac{1 + Bi_c \xi(t)}{\exp\left[-\alpha(\xi(t))^2\right]}\right] \tag{39}$$

Substitution of Eq. 39 in Eq. 34 gives a relationship between the local moisture content and the dry zone normalized thickness:

$$X(z,t) = \overline{X}_o \left[1 - \left[1 - \frac{z - L\xi(t)}{\frac{2\rho_s \overline{X}_o D_{le}}{\dot{m}_l} \frac{1 + Bi_c \xi(t)}{\exp\left[-\alpha(\xi(t))^2\right]}}\right]^2\right] \tag{40}$$

Similarly, substitution of Eq. 39 in Eq. 35 yields:

$$\overline{X} = \overline{X}_o \left(1 - \left[\xi(t) + \frac{2}{3}\frac{\rho_{dr} D_{le} \overline{X}_o}{\dot{m}_l L}\left(\frac{1 + Bi_c \xi(t)}{\exp\left[-\alpha(\xi(t))^2\right]}\right)\right]\right) \tag{41}$$

Equations 40 and 41 show that during the penetration period, both the local moisture content and the mean moisture content are dependent on the initial moisture content and on the drying rate during the constant rate period. For algebraic convenience, let us write:

$$u = \exp\left[\alpha[\xi(t)]^2\right] + Bi_c \xi(t) \exp\left[\alpha[\xi(t)]^2\right] \tag{42}$$

then, Eq. 41 becomes:

$$\overline{X} = \overline{X}_o(1 - [\xi(t) + Mu]) \tag{43}$$

with:

$$M = \frac{2}{3}\frac{\rho_{dr} D_{le} \overline{X}_o}{\dot{m}_l L} \tag{44}$$

For a slab being dried by one side, the drying rate in the falling rate period is defined as:

$$\dot{m} = -\rho_{dr} L \frac{d\overline{X}}{dt} \tag{45}$$

Substitution of Eqs. 29 and 43 in Eq. 45 yields:

$$\frac{\dot{m}_l}{u} = \rho_{dr} L \overline{X}_o \frac{d}{dt}(\xi(t) + Mu) \tag{46}$$

After some modifications, Eq. 46 becomes:

$$\frac{\dot{m}_l}{\rho_{dr} L \overline{X}_o} dt = \exp\left[\alpha[\xi(t)]^2\right] d\xi(t) + \frac{1}{2\alpha} \times Bi_c d\left\{\exp\left[\alpha[\xi(t)]^2\right]\right\} + \frac{M}{2} du^2 \tag{47}$$

Integration of Eq. 47 yields a relationship between the dry region normalized thickness and time during the regular regime:

$$t = t_{cr} + \frac{\rho_{dr} L \overline{X}_o}{\dot{m}_l}\left\{Lot(\alpha\xi(t)) + \frac{1}{2\alpha} Bi_c\left[\exp\left[\alpha\xi(t)^2\right] - 1\right] + \frac{M}{2}\left[\left(\exp\left[\alpha\xi(t)^2\right] + Bi_c\xi(t)\exp\left[\alpha\xi(t)^2\right]\right)^2 - 1\right]\right\} \tag{48}$$

where (see Appendix):

$$\mathrm{Lot}[\alpha\xi(t)] = \int_0^{\xi(t)} \exp\left[\alpha[\xi(t)]^2\right] \mathrm{d}\xi(t) \tag{49}$$

The time at the transition between the CDRP and the falling drying rate period for thick slabs is expressed as (Derdour et al.[25]):

$$t_{cr} = \frac{3}{2} D_{le}\left(\rho_{dr}\overline{X}_o/\dot{m}_l\right)^2 \tag{50}$$

Equation 48 allows one to determine the dry region normalized thickness as a function of time. Then Eqs. 39, 40, 41, and 29 allow the determination of respectively, the diffusional region thickness, the local moisture content, the mean moisture content, and the drying rate.

Transition Between the Penetration Period and the Regular Regime. At the end of the penetration period, the diffusional region thickness is equal to the material thickness, hence:

$$L = L\xi(t) + \frac{2\rho_{dr} D_{le} \overline{X}_o}{\dot{m}_l}\left[\frac{1 + Bi_c\xi(t)}{\exp\left[-\alpha(\xi(t))^2\right]}\right] \tag{51}$$

Combination of Eq. 51 with Eq. 48 yields the time corresponding to the transition between the penetration period and the regular regime, namely t_{tr}.

The Regular Regime. The internal moisture profile in the wet region during the entire falling rate period is given by the following equation obtained in Derdour et al.[23]:

$$X(z,t) = b(t)\left[(e(t) - L)^2 - (z - L)^2\right] \tag{52}$$

Substitution of Eq. 52 in Eq. 37 yields:

$$\dot{m} = -2\rho_{dr} D_{le} L b(t)(\xi(t) - 1) \tag{53}$$

Comparison of Eq. 29 with Eq. 53 gives the expression of the moisture profile curvature coefficient:

$$b(t) = -\frac{\dot{m}_l}{2\rho_{dr} D_{le} L}\frac{\exp\left(-\alpha[\xi(t)]^2\right)}{(1 + Bi_c\xi(t))(\xi(t) - 1)} \tag{54}$$

Substitution of Eq. 54 in Eq. 52 yields the expression of the local moisture content in the wet zone during the regular regime for thick products:

$$X(z,t) = -\frac{\dot{m}_l L}{2\rho_{dr} D_{le}}\frac{\exp\left[-\alpha[\xi(t)]^2\right]}{(1 + Bi_c\xi(t))(\xi(t) - 1)} \times \left[(\xi(t) - 1)^2 - (z/L - 1)^2\right] \tag{55}$$

During the regular regime, the mean moisture content expression was determined by Derdour et al.[23]:

$$\overline{X} = -\frac{2}{3} L^2 b(t)(\xi(t) - 1)^3 \tag{56}$$

Substitution of Eq. 54 in Eq. 56 yields the expression of the mean moisture content:

$$\overline{X} = \frac{\dot{m}_l L}{3\rho_{dr} D_{le}}\frac{(\xi(t) - 1)^2 \exp\left(-\alpha[\xi(t)]^2\right)}{1 + Bi_c\xi(t)} \tag{57}$$

Equations 55 and 57 show that during the regular regime, unlike during the penetration period, the local moisture content and the mean moisture content are not dependent on the initial moisture content. However, the drying rate during the CDRP still has an influence on these two variables.

Substitution of Eqs. 29 and 57 in Eq. 45, after few algebraic changes, yields:

$$dt = -\frac{L^2}{3D_{le}} \times \left[\frac{\left[2(\xi(t) - 1) - 2\alpha\xi(t)(\xi(t) - 1)^2\right](1 + Bi_c\xi(t)) - Bi_c(1 - \xi(t))^2}{1 + Bi_c\xi(t)}\right] \times d\xi(t) \tag{58}$$

After few modifications, Eq. 58 becomes:

$$dt = -\frac{L^2}{3D_{le} Bi_c^5} \times \begin{bmatrix} A_1 Z^3 + (Bi_c A_2 - 4A_1)Z^2 + (6A_1 - 3Bi_c A_2 + Bi_c^2 A_3)Z \\ -4A_1 + 3Bi_c A_2 - 2Bi_c^2 A_3 + Bi_c^3 A_4 \\ + \dfrac{\left\{A_1 - Bi_c A_2 + Bi_c^2 A_3 - Bi_c^3 A_4 + Bi_c^5 A_5\right\}}{Z} \end{bmatrix} dZ \tag{59}$$

with:

$$Z = 1 + Bi_c\xi(t) \tag{60}$$

and:

$$\begin{cases} A_1 = -2\alpha Bi, \\ A_2 = 2\alpha(1 - 2Bi_c), \\ A_3 = 4\alpha - 2Bi_c(\alpha - 1) - Bi_c, \\ A_4 = 2(1 - \alpha), \\ A_5 = -(2 + Bi_c) \end{cases} \tag{61}$$

Integration of Eq. 58 gives:

$$t = t_{tr} - \frac{L^2}{3D_{le}Bi_c^5} \times \left\{ \begin{array}{l} \frac{A_1}{4}\left[(1 + Bi_c\xi(t))^4 - \left(1 + Bi_c\xi(t)_{tr}\right)^4\right] \\ \quad + \frac{M_1}{3}\left[(1 + Bi_c\xi(t))^3 - \left(1 + Bi_c\xi(t)_{tr}\right)^3\right] \\ + \frac{M_2}{2}\left[(1 + Bi_c\xi(t))^2 - (1 + Bi_c\xi(t)_{tr})^2\right] \\ \quad + M_3Bi_c\left(\xi(t) - \xi(t)_{tr}\right) \\ + M_4\left[\ln(1 + Bi_c\xi(t)) - \ln\left(1 + Bi_c\xi(t)_{tr}\right)\right] \end{array} \right\} \tag{62}$$

with:

$$\begin{cases} M_1 = Bi_cA_2 - 4A_1 \\ M_2 = 6A_1 - 3Bi_cA_2 + Bi_c^2A_3 \\ M_3 = -4A_1 + 3Bi_cA_2 - 2Bi_c^2A_3 + Bi_c^3A_4 \\ M_4 = A_1 - Bi_cA_2 + Bi_c^2A_3 - Bi_c^3A_4 + Bi^4A_5 \end{cases} \tag{63}$$

Equation 62 allows determining the dry region normalized thickness for any given time, then knowing the $\xi(t)$ value, Eqs. 55, 57, and 29 allow calculating respectively the local moisture content, the mean moisture content, and the drying rate during the regular regime for thick products.

Modeling of the internal moisture distribution for thin products.

Regular Regime. For thin products, the entire falling rate period corresponds to the regular regime, thus, Eq. 62 simplifies to:

$$t = t_{cr} - \frac{L^2}{3D_{le}Bi_c^5} \times \left\{ \begin{array}{l} \frac{A_1}{4}\left[(1 + Bi_c\xi(t))^4 - 1\right] + \frac{M_1}{3}\left[(1 + Bi_c\xi(t))^3 - 1\right] \\ \quad + \frac{M_2}{2}\left[(1 + Bi_c\xi(t))^2 - 1\right] \\ + M_3Bi_c\xi(t) + M_4\ln(1 + Bi_c\xi(t)) \end{array} \right\} \tag{64}$$

where the duration of the CDRP in the case of thin slabs is expressed as (Derdour et al.[25]]:

$$t_{cr} = \frac{\rho_{dr}L\overline{X}_o}{\dot{m}_l} - \frac{L^2}{3D_{le}} \tag{65}$$

Here again, Eq. 64 represents a relationship between the dry region normalized thickness and time for thin slabs. Resolution of this equation permits determining $\xi(t)$ and thus, Eqs. 55, 57, and 29 give respectively for thin products, the local moisture content, the average moisture content, and the drying rate during the regular regime for thin slabs.

Calculation of the Drying Rate During the Constant Rate Period and the Convective Heat Transfer in the External Film. To be solved, the model needs the calculation of the drying rate during the constant rate period for any given set of drying conditions. This variable was calculated using the following expression obtained experimentally by Derdour[24] for drying of plaster for air temperatures ranging from 40°C to 80°C and air velocities from 1 to 5 m/s:

$$\dot{m}_l = 0.823 \times 10^{-6}(T_a^{1.39}V_a^{0.817}) \tag{66}$$

Then, the heat transfer coefficient, which combines convective transfer from air and heat transfer by radiation from the dryer walls, is easily deduced from Eq. 14:

$$h = \frac{\dot{m}_lL_v}{T_a - T_w} \tag{67}$$

The critical moisture content is calculated using the following expressions obtained previously Keey,[5] Suzuki,[27] and by Derdour et al.[25]:

For thick products:

$$\overline{X}_{cr} = \overline{X}_o\left[1 - \frac{2}{3}\frac{\rho_{dr}D_{le}\overline{X}_o}{\dot{m}_lL}\right] \tag{68}$$

For thin products:

$$\overline{X}_{cr} = \frac{\dot{m}_lL}{3\rho_{dr}D_{le}} \tag{69}$$

Materials and Methods

To check the validity of the model, experimental internal moisture distributions during the DDRP were measured for four sets of drying conditions of plaster slabs. This product which was provided by Lafarge (Saint Quentin Fallavier, France) is used as a humidity regulator in buildings. Thus the knowledge of the moisture transport mechanism within this product is important. Plaster presents the two main drying periods and does not shrink during drying. Its desorption isotherm was determined (cf. Figure 3) and indicates that plaster behaves as a nonhygroscopic product in the range of the spanned drying conditions. Finally, its porous structure respects the model assumptions. The physico-chemical characteristics of the plaster used are presented on Table 1.

The experiments were carried out in a tunnel dryer with air regeneration (cf. Figure 4). The dryer is equipped so as to permit the control of the air temperature and velocity. The absolute air humidity was kept constant for all the experiments. The sample was flat and placed on a hollow tray so that it was in contact with the air only with one face. The other face is insulated permitting a one directional heat and mass transfer and minimal heat losses. The drying rates were kept equal or more than 0.0003 kg/m^2 s, so that the model predicting the critical moisture content was applicable (Derdour et al.[25]). Air characteristics were temperatures of 70°C and 80°C and velocities of 2 and 3 m/s. Vapor partial pressure in air was kept constant and equal to 850 Pa. Under those drying conditions, as the equilibrium moisture content is always approximately nil.

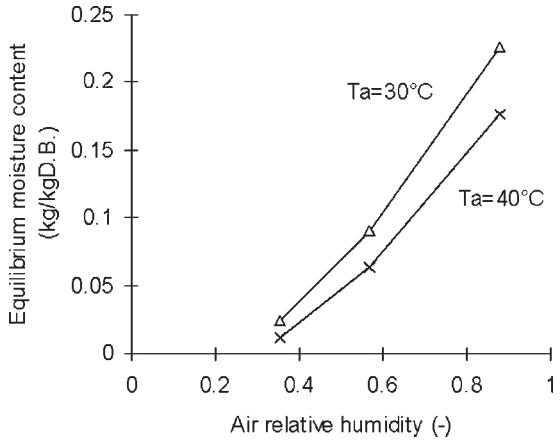

Figure 3. Desorption isotherm of plaster.

Therefore, the product can be considered as nonhygroscopic in the range of drying conditions investigated.

The experimental internal moisture distributions were measured by removing the sample after a certain time during the falling drying rate period, slicing it into four parts, then measuring the moisture content in each part by a gravimetric method: The slices are weighed and placed in an oven at 50°C, 1 atm, and 2% humidity for several days until their weight becomes constant. These experiments were carried out only with 3-cm thick samples. For thinner samples, it was practically impossible, with our means, to slice them into four parts of equal thicknesses.

Results and Discussion

Figures 5–8 show the experimental and the predicted internal moisture distributions for four sets of drying conditions. Table 2 provides predicted and experimental values of $\overline{X}_{cr}$ and t_{cr} for the experiments reported. Figures 5–8 show some nonnegligible deviations between the model predictions and the experimental values in the liquid diffusion zone. To better assess the validity of the model predictions, a statistical treatment of the experimental results and the model's calculations in the liquid diffusion zone was realized. The mean relative differences (MRDs) between the experimental internal moisture content and the predicted values were calculated. The results are gathered in Table 3. The results obtained for the experiment at 80°C and 2 m/s appear to be affected by large errors, which are due to a possible experimental error or an instrumental failure during that particular experiment. A Q-test

Table 1. Characteristics of the Product

Property/Parameter	Value
Effective thermal conductivity: λ_{eff} (W/mK) (Derdour[24])	0.67
Bulk density: ρ_{dr} (kg/m^3) (Derdour[24])	1162
Initial moisture content: $\overline{X}_o$ (kg/kg$_{D.B.}$)	0.34
Internal moisture diffusivity: D_{le} (m^2/s) (Derdour et al.[25])	3.6×10^{-9}
Heat transfer importance coefficient: α (Derdour[24])	12

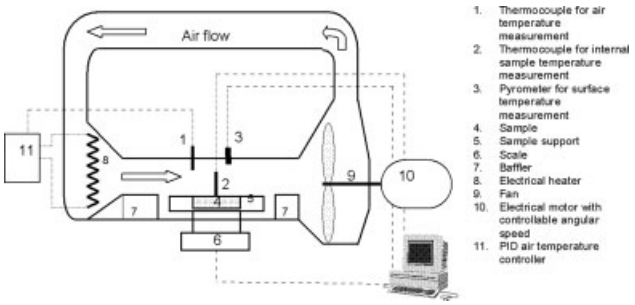

Figure 4. Experimental dryer.

was run for that particular experiment and it suggests that this result should be discarded. Therefore, results from that experiment were not considered in the interpretation of the experimental data.

The MRD between the calculated internal moisture content and the experimental values for the penetration period is 27% indicating significant discrepancies between the model calculations and the experimental data. On the other hand, the MRD calculated for the regular regime is 29% showing that the calculations also do not lie within an acceptable range with the experimental data. The probable causes of the model calculations deviations from the experimental measurements are as follows:

1. A non-negligible variation of the moisture diffusion coefficient in the liquid zone during the penetration period which is not accounted for in the model formulation;

2. The measured local moisture content represents the mean moisture content of the slice and is attributed to the center of the slice. The calculated moisture content at the middle of the slice is not equal to the mean moisture content of the slice if the moisture content profile is not linear;

3. The moisture transport from inside the slice to external surfaces followed by evaporation; This is due to the heat of friction that is generated during the slicing operation which

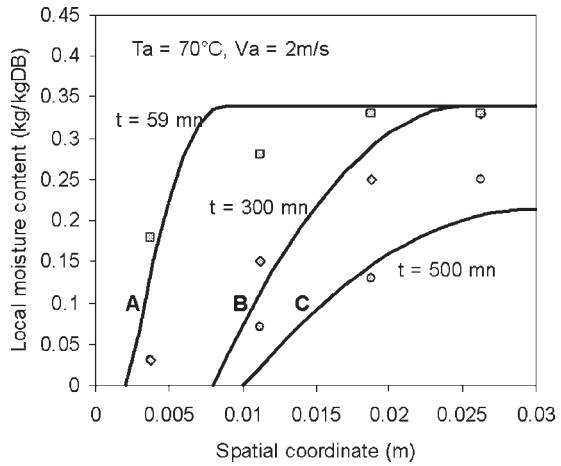

Figure 5. Internal moisture content during the falling rate period.

Comparison between experimental results and model's predictions (T_a = 70°C, V_a = 2 m/s). A and B: Penetration period: $t_{cr} < t < t_{tr}$; C: Regular regime: $t > t_{tr}$.

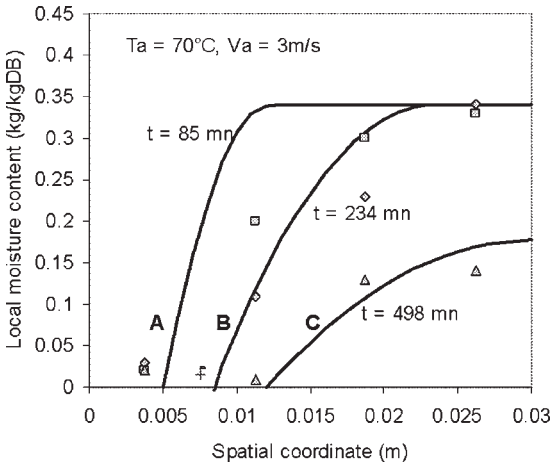

Figure 6. Internal moisture content during the falling rate period.

Comparison between experimental results and model's predictions (T_a = 70°C, V_a = 3 m/s). A and B: Penetration period: $t_{cr} < t < t_{tr}$; C: Regular regime: $t > t_{tr}$.

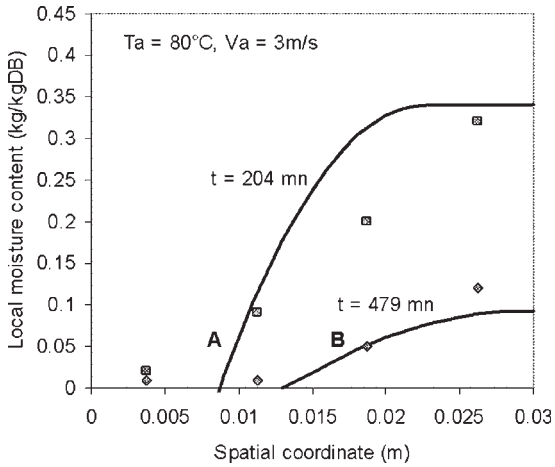

Figure 8. Internal moisture content during the falling rate period.

Comparison between experimental results and model's predictions (T_a = 80°C, V_a = 3 m/s). A: Penetration period: $t_{cr} < t < t_{tr}$; B: Regular regime: $t > t_{tr}$.

takes 5–10 min to be achieved. This transport occurs readily for high internal moisture gradients, which are expected to exist in the liquid diffusion zone.

In contrast, experimental internal moisture content values indicate that by the late stages of drying (when the mean moisture content approaches zero and the product external surface temperature approaches air temperature) liquid moisture tends to migrate into the dry zone. This observation can be explained by the existence of another transport mechanism occurring at high temperatures, which characterize the late stages of drying. The mechanism more likely to occur at high temperatures is thermodiffusion, which was first introduced by Luikov.[17] This mechanism contributes to liquid transport at high temperatures and its driving force is the temperature gradient, which characterizes materials with low thermal conductivity. At high temperature gradients, thermodiffusion facilitates a liquid migration inside the zone already dried.

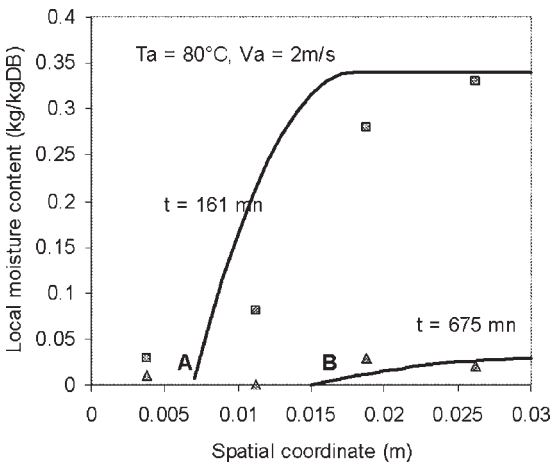

Figure 7. Internal moisture content during the falling rate period.

Comparison between experimental results and model's predictions (T_a = 80°C, V_a = 2 m/s). A: Penetration period: $t_{cr} < t < t_{tr}$; B: Regular regime: $t > t_{tr}$.

Furthermore, the temperature at the receding evaporative front becomes close to the temperature of the bottom insulation at the end stages of drying. This temperature is different from the mean temperature since the product has a low thermal conductivity (at this stage the temperature of the external surface is close to air temperature). This deviation from the model's hypothesis has a certain contribution in the differences observed between the experimental internal moisture contents and the model's predictions at the late stages of drying. Nevertheless, these errors tend to be insignificant toward the end of drying during which only about 5% of initial moisture content remains in the product.

Experimental errors associated with the moisture content measurement are also believed to contribute to the differences between the experimental results and the model predictions at low internal moisture contents when the relative error becomes important (more than 50%). The absolute error of the internal moisture content measurement was evaluated as 0.04 kg/kg_{DB} depending on the instrumentation and the operation of slicing the sample.

Prediction of the evolution of the dry zone was also assessed. Experimental moisture contents lower than the absolute error associated with the measurement (0.04 kg/kg_{DB}) can be considered as indicating a dry sample and thus indicate the experimentally observed evolution of the dry zone. Comparison of the model's predictions of the evolution of the dry zone with the experimental data indicate that the calculations of the

Table 2. Values of $\overline{X}_{cr}$ and t_{cr} for the Experiments Reported ($\overline{X}_{cr}$ and t_{cr} are reported in kg/kg_{DB} and s, respectively)

	$\overline{X}_{cr\text{-}mod}$	$t_{cr\text{-}mod}$	$\overline{X}_{cr\text{-}exp}$	$t_{cr\text{-}exp}$
T_a = 80°C; V_a = 2m/s	0.32	912	0.33	834
T_a = 80°C; V_a = 3m/s	0.33	470	0.33	384
T_a = 70°C; V_a = 2m/s	0.32	1323	0.31	1440
T_a = 70°C; V_a = 3m/s	0.33	682	0.32	654

Table 3. Statistical Treatment of the Experimental Results for the Liquid Diffusion Region

Air temperature (°C)	70	70	80	80
Air velocity (m/s)	2	3	2	3
Average RD *(%)	29	29	65	27
s †(−)	21.6	22.2	57.7	24.8
RD_{max} (%)	71	65	163	60

*The relative difference calculated between the model prediction and the experimental moisture content: $RD = 100\left|(X_{exp} - X_{mod})/X_{exp}\right|$.

†The estimated standard deviation of the relative difference: $s = \sqrt{\frac{\sum_{l=1}^{l=N}(RD_l - RD)^2}{N-1}}$.

thickness of the dry zone fall within an acceptable range with the experimental results.

Nevertheless, from the light of the experimental data, it appears that, overall, the analytical model presented in this article fails to provide a reliable and accurate prediction of the local moisture content in the liquid diffusion zone. However, relatively few experimental data were used to access the model validity and the experimental method employed is suspected to induce large experimental errors. Therefore, more experimental data obtained with a more reliable, nondestructive, and online methods will certainly better access the validity and the limits of the model presented in this article.

Conclusions

In this study, a model for the prediction of internal moisture content distribution for porous nonhygroscopic thin slabs was determined. This model is based on the assumption of the existence of a receding evaporative front within the product during the falling drying rate period. Heat transfer in the dry zone is considered to be the limiting process. Relative difference between calculated internal moisture contents and experimental data obtained on plaster slabs was found to be ~29%, which is rather a mediocre prediction. This deviation is attributed to a variation of the liquid moisture diffusion coefficient and to the destructive experimental method. Experimental results showed that the regular regime always occurs during drying of porous nonhygroscopic slabs. The thickness of the dry zone is well predicted by the product. Finally, for very low internal moisture content and high temperatures, experimental results indicate a liquid transport into the dried zone. This observation is probably due to the occurrence of thermodiffusion resulting from the increase in internal temperature gradients during the end stages of drying. Confrontation of the model's prediction with experimental results obtained a more reliable method will provide a better assessment of the model's validity and limits.

Acknowledgments

The authors are very grateful to Lafarge, Saint Quentin Fallavier, France, for generously providing test materials and technical collaboration.

Notation

A_e = surface of evaporation (m^2)
b(t) = moisture content gradient curvature coefficient ($kg/kg_{DB}/m^2$)
Bi_c = heat Biot number
Bi_m = mass Biot number
Cp = mass thermal capacity [J/(kg K)]
D_{le} = liquid diffusion coefficient (m^2/s)
D_v = vapor diffusion coefficient (m^2/s)
$e(t)$ = thickness of the dry zone (m)
h = convective heat transfer coefficient in external film [$W/(m^2 K)$]
L = product thickness (m)
L_{lim} = transitional thickness between thick and thin products (m)
L_v = heat of water vaporization (J/kg)
$\dot{m}$ = drying rate [$kg/(m^2 s)$]
$\dot{m}_l$ = drying rate during the constant drying rate period [$kg/(m^2 s)$]
P = pressure (Pa)
q = fraction of heat absorbed by the product
Q_{trans} = amount of heat transferred to the product (J)
Q_{prod} = amount of heat used to elevate the product temperature (J)
Q_{evap} = amount of heat used to evaporate moisture (J)
R = universal constant of ideal gases (J)
RD = relative difference between the calculated moisture content and the experimental value [J/(mol K)]
s = estimated standard deviation
T = temperature (°C)
T_w = wet bulb temperature (°C)
t = time (s)
V = volume (m^3)
$\underline{X}$ = local moisture content reported to the dry basis (kg/kg_{DB})
$\overline{X}$ = mean moisture content reported to the dry basis (kg/kg_{DB})
z = spatial coordinate (m)

Greek letters

α = heat transfer importance coefficient
α_{VB} = Van Brakel proportionality constant, Eq. 25 (s)
λ_{dr} = thermal conductivity of the dry zone (W/m s)
ρ_{dr} = density of the dry zone (kg/m^3)
$\xi(t)$ = dry zone normalized thickness
$\gamma(t)$ = thickness of the diffusionnal region (m)
Γ = dimensionless number, Eq. 11
Ψ = dimensionless number, Eq. 16
Ω = dimensionless number, Eq. 17
Λ = dimensionless number, Eq. 21

Subscripts

a = related to the air
cr = at the critical point
tr = at the transition between the penetration period and the regular regime
dr = related to the dry region (dry product)
e = related to the evaporative front
exp = experimental value or related to the experience
ht = related to heat transfer
I = during the constant rate period
mod = calculated using the model
mt = related to heat transfer
prod = relative to the product (average value)
o = at the beginning of the drying
s = at the external surface of the product
v = related to the vapor

Literature Cited

1. Bindschaedler C. Lyophillization process validation, drug and the pharmaceutical sciences. In: Rey L, May JC, editors. *Freeze-Drying/Lyophilization of Pharmaceutical and Biological Products*, 2nd ed. New York: Marcel Dekker, 1999:373–408.
2. May CJ. Regulatory control of freeze-dried products: importance and evaluation of residual moisture, drug and the pharmaceutical sciences. In: Rey L, May JC, editors. *Freeze-Drying/Lyophilization of Pharmaceutical and Biological Products*, 2nd ed. New York: Marcel Dekker, 1999:199–230.
3. Hancock BC, Zografi G. Characteristics and significance of the amorphous state in pharmaceutical systems. *J Pharm Sci*. 1999;86:1–12.
4. Martynenko OG, Pavlyukevich NV, Rudin GI. Mathematical methods and kinetics of heat and mass transfer with phase change in porous

media. In: Mujumdar AS, editor. *Advances in Drying, Vol. 1*. New York: Hemisphere, 1980:101–118.
5. Keey RB. *Introduction to Industrial Drying Operations*. New York: Pergamon, 1978.
6. Schlünder EU. Dryers. In: *Heat Exchanger Handbook*. Schlünder EU, editor, New York: Hemisphere, 1983.
7. Van Brakel J. Mass transfer in convective drying. In: Mujumdar AS, editor. *Advances in Drying, Vol. 1*. New York: Hemisphere, 1980: 217–267.
8. Coumans WJ. Models for drying kinetics based on drying curves of slabs. *Chem Eng Process*. 2000;39:53–68.
9. Belhamri A. Characterization of the first falling rate period during drying of porous material. *Drying Technol*. 2003;21:1235–1252.
10. Derdour L, Desmorieux H. A model for internal moisture diffusivity comparison with experimental data obtained on plaster and spirulina. In: Mujumdar AS, editor. *Proceedings of the 14th International Drying Symposium, Vol. A*; Campinas: Ouragraf Grafica e Editora. 2004:718–725.
11. Pel L, Landman KA. A sharp drying front model. *Drying Technol*. 2004;22:637–647.
12. Marinos-Kouris D, Maroulis ZB. Transport properties in the drying of solids. In: Mujumdar AS, editor. *Handbook of Industrial Drying*, 2nd ed. New York: Marcel Dekker, 1995; Vol. 1:113–159.
13. Chen G, Wang W. Mathematical modeling of solids drying. A comprehensive review. *Proceedings of the 3rd Inter-American Drying Conference*. 2005: Paper K-1.
14. Crank J. *The Mathematics of Diffusion*. Oxford: Clarendon, 1975.
15. Moyne C, Roques M, Wolf W. *A collaborative experiment of drying beds of glass spheres. Physical Properties of Foods 2*. New York: Elsevier Applied Science, 1989:27–48.
16. De vries DA. Simultaneous transfer of heat and moisture in porous media. *Trans Am Geophys Union*. 1958;39:909–915.
17. Luikov AV. Systems of differential equations of heat and mass transfer in capillary porous bodies. *Int J Heat Mass Transfer*. 1975;18: 1–14.
18. Peishi Chen P, Pei D. A mathematical model of drying processes. *Int J Heat Mass Transfer*. 1989;32:297–310.
19. Schadler N, Kast K. A complete model of the drying for porous bodies. Experimental and theoretical studies. *Int J Heat Mass Transfer*. 1987;30:2031–2044.
20. King CG. *Freeze Drying of Foods*. Boca Raton: Chemical Rubber, 1971.
21. Rey LR. Glimpses into the realm of freeze-drying: classical issues and new ventures. In: Rey L, May JC, editors. *Freeze-Drying/Lyophilization of Pharmaceutical and Biological Products*, 2nd Ed. New York: Marcel Dekker, 1999:1–30.
22. Mujumdar AS, Menon AS. Drying of solids: principles, classification and selection of dryers. In: Mujumdar AS, editor. *Handbook of Industrial Drying*, 2nd ed. New York: Marcel Dekker, 1995; Vol. 1:1–39.
23. Derdour L, Desmorieux H, Andrieu J. A contribution to the characteristic drying curve concept Application to the drying of plaster. *Drying Technol*. 2000;18:237–260.
24. Derdour L. Contribution to the characteristic drying curve concept. Application to plaster-based materials. PhD Thesis, University of Lyon I, France, 1998.
25. Derdour L, Desmorieux H, Andrieu J. Determination and interpretation of the critical moisture content (C.M.C.) and the internal moisture content profile during the constant rate period. *Drying Technol*. 1998;16:813–824.
26. Keey RB, Suzuki M. On the characteristic drying curve. *Int J Heat Mass Transfer*. 1974;17:1455–1464.
27. Suzuki M. Prediction of critical moisture content. In: Mujumdar AS, editor. *Proceedings of the 2nd International Drying Symposium*. New York: Hemisphere, 1980:116–127.

Appendix

Evolution of the ratio $P_{ve}(t)/T_e(t)$ for water

Figure A1 shows the evolution of the ratio $P_{ve}(t)/T_e(t)$ for water in the range of air temperatures comprised between 20°C and 100°C.

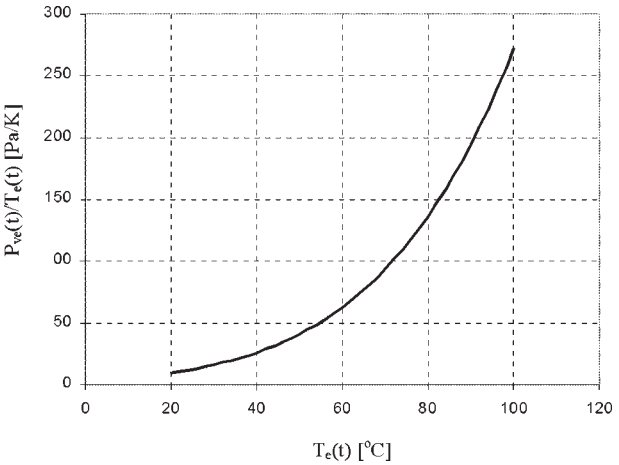

Figure A1. $P_{ve}(t)/T_e(t)$ vs. $T_e(t)$ for water.

Integrating Lot[$\alpha\xi(t)$]

Let us recall the expression of Lot[($\alpha\xi(t)$]:

$$\mathrm{Lot}(\alpha\xi(t)) = \int_0^{\xi(t)} \exp\left[\alpha(\xi(t))^2\right] d\xi(t) \qquad \text{(A1)}$$

Integration by parts gives an infinite sum that writes:

$$\mathrm{Lot}(\alpha\xi(t)) = \sum_{i=0}^{\infty} \frac{(-1)^i (2\alpha)^j}{\prod_{j=0}^{i}(2j+1)} \left[\xi(t)\right]^{2i+1} \exp\left[\alpha(\xi(t))^2\right] \qquad \text{(A2)}$$

Since α is a real number and $\xi(t)$ value is between 0 and 1, the sum above converges and it is equal to a real value. For plaster, the variation of Lot($\alpha.\xi(t)$) was determined and it is given on Figure A2.

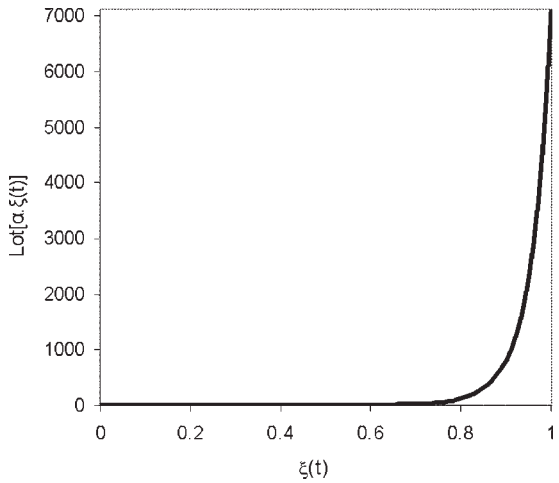

Figure A2. Lot[$\alpha\xi(t)$] as a function of $\xi(t)$. (Case of plaster, $\alpha = 12$).

Manuscript received Oct. 20, 2006, revision received Aug. 31, 2007, and final revision received Oct. 19, 2007.